Nano Research
2020, 13(2): 353–357
ISSN 1998-0124 CN 11-5974/O4
https://doi.org/10.1007/s12274-020-2613-3

Research Article

A non-rigid shift of band dispersions induced by Cu intercalation in 2H-$TaSe_2$

Pengdong Wang[1,§], Rashid Khan[1,§], Zhanfeng Liu[1], Bo Zhang[1], Yuliang Li[1], Sheng Wang[1], Yunbo Wu[1], Hongen Zhu[1], Yi Liu[1], Guobin Zhang[1], Dayong Liu[2], Shuangming Chen[1] (✉), Li Song[1] (✉), and Zhe Sun[1,3,4] (✉)

[1] *National Synchrotron Radiation Laboratory, University of Science and Technology of China, Hefei 230029, China*
[2] *Key Laboratory of Materials Physics, Institute of Solid State Physics, Chinese Academy of Sciences, P. O. Box 1129, Hefei 230031, China*
[3] *Key Laboratory of Strongly-coupled Quantum Matter Physics, Chinese Academy of Sciences, University of Science and Technology of China, Hefei 230026, China*
[4] *CAS Center for Excellence in Superconducting Electronics (CENSE), Shanghai 200050, China*
[§] *Pengdong Wang and Rashid Khan contributed equally to this work.*

Received: 12 August 2019 / **Revised:** 14 December 2019 / **Accepted:** 18 December 2019

ABSTRACT

The intercalation of metal is a promising method for the modulating electronic properties in transition metal dichalcogenides (TMDs). However, there still lacks enough knowledge about how the intercalated atoms directly impact the two-dimensional structural layers and modulate the band structures therein. Taking advantage of X-ray absorption fine structure and angle-resolved photoemission spectroscopy, we studied how Cu intercalation influences the host $TaSe_2$ layers in $Cu_{0.03}TaSe_2$ crystals. The intercalated Cu atoms form bonds with Se of the host layers, and there is charge transfer from Cu to Se. By examining the changes of band dispersions, we show that the variation of electronic structures is beyond a simple rigid band model with merely charge doping effect. This work reveals that the unusual change of band dispersions is associated with the formation of bonds between the intercalated metal elements and anion ions in the host layers, and provides a reference for the comprehensive understanding of the electronic structures in intercalated materials.

KEYWORDS

transition metal dichalcogenides, Cu-intercalation, band shift, angle resolved photoemission spectroscopy

1 Introduction

Transition metal dichalcogenides (TMDs) are quasi-two-dimensional layered compounds with abundant physical phenomena such as superconductivity, metal-insulator transition, charge density wave, and many other electronic and optical properties [1–4]. Their physical and chemical characteristics could be tuned with various approaches, including chemical doping, vacancies, intercalation [5–7]. Owing to the weak coupling between neighboring layers, the intercalation procedure can introduce foreign species into the van der Waals gap. By this means, the main physics in the functional host layers could be easily altered by manipulating charge doping or the coupling between adjacent layers with different interlayer spacing.

Generally speaking, the primary effect of the intercalation of metal elements is to increase the carrier concentration and realize electron doping in the host systems. This doping approach is able to result in new physical properties in the host layers. For example, in semiconducting materials, extra electrons provided by intercalated atoms fill in the bottom of conduction bands and thus induce metallic characteristics [8]. In Cu-intercalated $TiSe_2$, electron doping by Cu intercalants suppresses charge-density-wave (CDW) phase and give rise to superconductivity [9, 10]. Li intercalation in MoS_2 provides extra electrons to MoS_2 layers and lead to a structural transition from 2H phase to 1T phase [11]. However, besides the versatile effects introduced by charge doping, there still lacks enough knowledge about how the intercalated atoms directly impact the two-dimensional structural layers and modulate the band structures therein.

Aiming to reveal the influence of intercalated ions on the host layers, we studied Cu-intercalated $TaSe_2$. In $TaSe_2$, there are multiple bands around the Fermi level, and three pockets can be identified on the Fermi surface [12–15]. By monitoring the change of electronic structures near the Fermi level, we are able to reveal whether intercalated atoms affect the band structures in the pristine two-dimensional structural layers. In our studies, X-ray absorption fine structure (XAFS) was employed to investigate the atomic configurations in the intercalated system. Our data show that, though the lattice structure of the pristine $TaSe_2$ remains basically the same after Cu intercalation, Cu ions do form bonds with Se anions in $TaSe_2$ layers. On the other hand, our ARPES data demonstrate that band dispersions along high symmetry directions in *k*-space vary in different ways, and the overall characteristics cannot be interpreted within a simple rigid band model as expected for merely charge doping effect. We attribute the change of band dispersions to the formation of Cu–Se bonding and the resulting charge transfer. Our studies show that the intrinsic band

Address correspondence to Zhe Sun, zsun@ustc.edu.cn; Li Song, song2012@ustc.edu.cn; Shuangming Chen, csmp@ustc.edu.cn

dispersions of host layers in van der Waals crystals could be tuned by atom intercalation when the foreign atoms form bonds with the anions of host layers.

2 Results and discussions

Our samples were grown using chemical vapor transportation (CVT) method. The stoichiometric amounts of Ta, Se, and Cu powders (purchased from Sigma-Aldrich) were mixed together for $TaSe_2$ and Cu-intercalated $TaSe_2$, with iodine as a transport agent. These materials were sealed into quartz ampoule tubes with inner diameter of 5 mm and length of 25 cm under a vacuum of 1×10^{-3} Torr. After sealing the quartz tubes were put into a two-zone furnace with the hot zone temperature of 950 °C and the growth zone temperature of 850 °C for five days. The furnace was then cooled down to room temperature, and single crystals of $TaSe_2$ and $Cu_{0.03}TaSe_2$ with size of a few millimeters were obtained. XAFS measurements were performed in the transmission mode at the beamline 14W1 in Shanghai Synchrotron Radiation Facility (SSRF). The X-ray was monochromatized by a double-crystal Si(311) monochromator. XAFS data were analyzed with the WinXAS3.1 program [16]. Theoretical amplitudes and phase-shift functions were calculated with the FEFF8.2 code [17]. ARPES measurements were performed at ARPES beamline (BL-13U) of National Synchrotron Radiation Laboratory, Hefei, with VG R4000 analyzer. The energy and angular resolutions are better than 20 meV and 0.3°, respectively. Single crystals of $TaSe_2$ and $Cu_{0.03}TaSe_2$ were cleaved in ultrahigh vacuum better than 7×10^{-11} Torr to achieve clean surfaces.

Figure 1(a) shows the crystal structures of 2H-$TaSe_2$, and Fig. 1(b) indicates the position of copper atoms in $Cu_{0.03}TaSe_2$. Copper atoms are intercalated into the van der Waals gap between neighboring $TaSe_2$ layers. Though the exact positions of individual Cu atoms cannot be identified, as will be shown in Fig. 2, our XAFS data indicate that Cu atoms are not randomly sitting between the $TaSe_2$ layers, and instead Cu–Se bonds take place in $Cu_{0.03}TaSe_2$. We note here that in our samples the Cu intercalation does not induce superlattice structures, as evidenced by the low energy electron diffraction (LEED) pattern in Fig. 1(c). This is distinct from the previous studies by Kordyuk et al., in which a superlattice structure arises in Cu-intercalated $TaSe_2$ and leads to a very different band structures from our data [18]. This difference could be due to the different sample synthesis processes and Cu concentration.

High-resolution transmission electron microscopy (HRTEM) was used to characterize the lattice parameters of $TaSe_2$ and $Cu_{0.03}TaSe_2$ single crystals. HRTEM images reveal the *d*-spacing of 0.270 nm for the periodic interlayer arrays of (104) in both $TaSe_2$ and $Cu_{0.03}TaSe_2$ single crystals (Figs. 1(d) and 1(e)). In order to investigate how Cu intercalants interact with $TaSe_2$ layers, we performed XAFS to examine the local chemical bonding in $Cu_{0.03}TaSe_2$. In Fig. 2(a), XAFS results show that, with the $TaSe_2$ as a reference, the absorption edge of Ta shifts to lower energies after Cu intercalation, indicating extra electrons provided by Cu were transferred to the $TaSe_2$ layers. Their Fourier transform spectra of extended XAFS (FT-EXAFS) curves indicate that the Ta–Se bond length remains the same (Fig. 2(b)), suggesting that the atomic configurations between Ta and Se is robust against Cu intercalation. We further examined the valence states of Cu in $Cu_{0.03}TaSe_2$. As shown in Fig. 2(c), the absorption edge of Cu in $Cu_{0.03}TaSe_2$ is very close to that of Cu foil, indicating that the charge transfer from Cu to $TaSe_2$ layers is not significant. The corresponding Fourier transform spectra indicate that Cu and the Se in $TaSe_2$ layers form chemical bonds with a bond length similar to that of CuSe (see Fig. 2(d)). These results suggest that the intercalated Cu atoms are not simply sitting in the van der Walls gap between neighboring $TaSe_2$ layers, and they do affect the electronic systems in $TaSe_2$ layers by forming chemical bonds with Se. The detailed structure parameters calculated from XAFS studies are summarized in Table 1. Therefore, it is natural to expect some changes in the band dispersions other than a simple charge doping. The structural analysis of XAFS results are in agreement with our HRTEM data.

To investigate how the Cu intercalation alters the electronic structures of $TaSe_2$ layers, we carried out ARPES measurements of these samples. In $Cu_{0.03}TaSe_2$, Cu atoms donate extra electrons into $TaSe_2$ layers and lead to a charge doping in the pristine

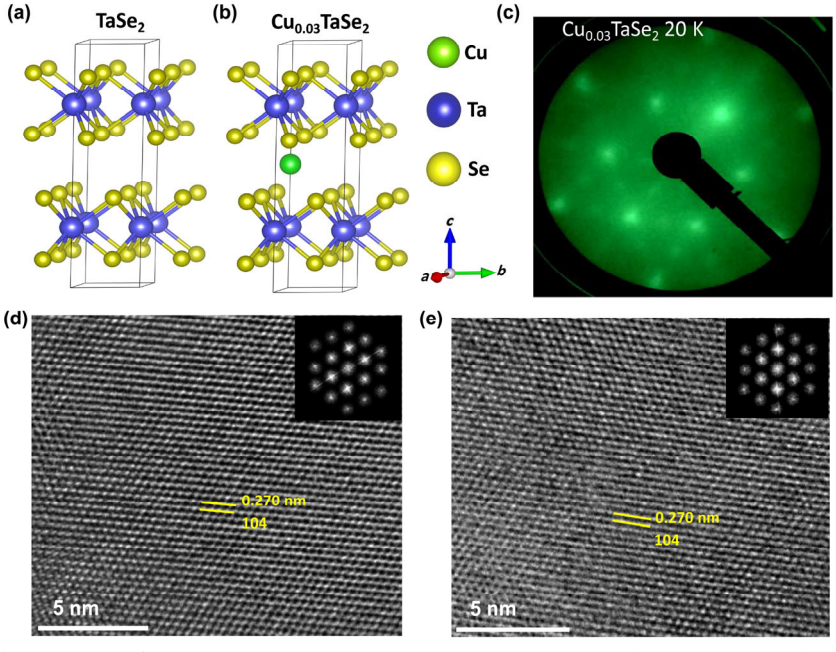

Figure 1 (a) Crystallographic structures of $TaSe_2$. Ta, Se and Cu atoms are represented by blue, yellow and green balls, respectively. (b) A schematic diagram for the intercalation position of copper atoms in $Cu_{0.03}TaSe_2$. (c) LEED pattern of $Cu_{0.03}TaSe_2$ taken at T = 20 K. (d) and (e) HRTEM images and corresponding Fast Fourier Transformation (FFT) pattern of $TaSe_2$ and $Cu_{0.03}TaSe_2$, respectively. No evident lattice shift was observed in FFT patterns.

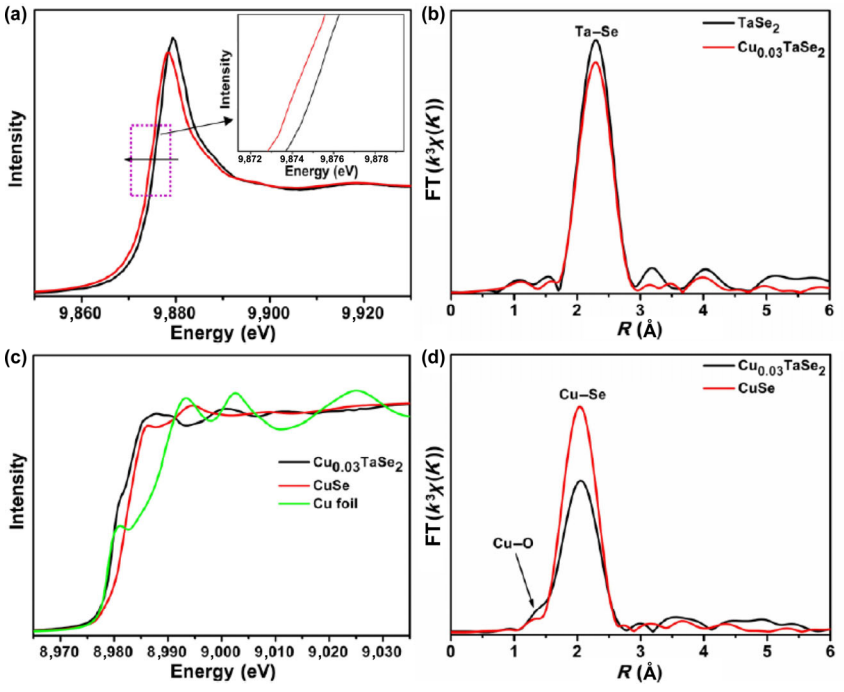

Figure 2 (a) Ta K-edge XANES spectra for the $TaSe_2$ and $Cu_{0.03}TaSe_2$ single crystals. (b) The corresponding Fourier transforms FT($k^3\chi(k)$) Ta–Se. (c) Cu K-edge XANES spectra for the $Cu_{0.03}TaSe_2$, CuSe and Cu foil. (d) The corresponding Fourier transforms FT($k^3\chi(k)$) Cu–Se. The shoulder is derived from Cu–O bond, which is introduced by the oxidation during the sample grinding process for XANES measurements.

Table 1 Structural parameters of $TaSe_2$, $Cu_{0.03}TaSe_2$ and CuSe

Samples	Bond	Coordination number N	Bond length	σ^2 (10^{-3} Å^2)
$TaSe_2$	Ta–Se	6	2.60	4.3
$Cu_{0.03}TaSe_2$	Ta–Se	5.9	2.60	4.6
	Cu–Se	3.4	2.39	8.9
CuSe	Cu–Se	4	2.37	7.5

electronic structures of $TaSe_2$. Generally speaking, such a charge doping is expected to suppress the CDW phase in the parent $TaSe_2$. In $TaSe_2$, the electronic structures become very complicated in below T = 90 K [19, 20], which is thus not suitable to serve as a reference to evaluate the variation of electronic structure in $Cu_{0.03}TaSe_2$. In order to eliminate the effect of CDW in $TaSe_2$, we performed ARPES measurements at T = 95 K, and the Fermi surface topology is shown in Fig. 3(a). For comparison, the data of $Cu_{0.03}TaSe_2$ is displayed in Fig. 3(b).

Previous ARPES measurements and theoretical calculations show that the electronic structure of $TaSe_2$ has quasi-two dimensional characteristics [21–24], which indicates that the k_z dispersions are relatively weak and the band dispersions probed by ARPES measurements are approximately independent of the photon energies. Meanwhile, the two-dimensionality of electronic structures in the intercalated crystals is also confirmed experimentally, as shown in Fig. 3(c), since the k_z dispersions are very weak. Therefore, when comparing the effect of Cu intercalation on the band dispersions of $TaSe_2$, we can ignore the k_z variation of electronic structures in both the parent and the intercalated compounds.

In Fig. 3, there are two evident changes. The pocket size around the center of the Brillouin zone is reduced in the intercalated crystals, and the shape of dog-bone pocket around M in 2H-$TaSe_2$ changes to rounded rectangle in the $Cu_{0.03}TaSe_2$. In addition, the pocket around K cannot be clearly identified in the intercalated samples. The pocket around the center of the Brillouin zone is a hole type. Its shrink in size suggests that intercalated Cu atoms contribute extra electrons to the $TaSe_2$ layers and lead to a rise of the Fermi level. In Fig. 4, we also show the ARPES intensity plots of 2H-$TaSe_2$ and $Cu_{0.03}TaSe_2$ along high symmetry directions in momentum space. It is evident that the overall electronic states in $Cu_{0.03}TaSe_2$ move to deeper binding energies, indicating an electron doping effect induced by Cu intercalation.

The change of pocket shape around M could arise either from the shift of the Fermi level caused by a charge doping, or from the change of band dispersions induced by the Cu intercalation. In order to find out whether the former case plays an important role, we show in Figs. 3(d)–3(i) the photoemission intensity at various constant energies taken from 2H-$TaSe_2$ and Cu-intercalated compound. One can notice that in both the parent and the intercalated samples, the different profiles of the Fermi pockets around M remain the same over a larger energy range, though the size changes as a function of binding energies. This behavior indicates that the shape change of Fermi surface pockets is not due to the charge doping effect. We thus argue that Cu intercalants are not only responsible for the shift of the Fermi level, but also accountable for the change of band dispersions in $Cu_{0.03}TaSe_2$.

Moreover, the different band structures are not related to the possible change of dimensionality after the Cu intercalation. One may expect that the intercalation could slightly increase the interlayer spacing, reduce the interlayer coupling and make the system more two-dimensional. In fact, ARPES studies on single-layer $TaSe_2$ have indicated that the Fermi surface of $TaSe_2$ on the two-dimensional limit still bears similarity to that of bulk $TaSe_2$ [25].

Figure 4 shows band dispersions of both $TaSe_2$ and $Cu_{0.03}TaSe_2$. In order to examine the variations of band structures induced by Cu intercalants, we plot the dispersions of $TaSe_2$ (red dashed lines) along high symmetry directions on the data of intercalated samples. One could notice that a simple rigid band shift is not suitable to account for the changes in dispersive features. In Figs. 4(a) and 4(d), along the Γ–K direction, though the dispersion is not clear on the right side for $Cu_{0.03}TaSe_2$, one can still notice that the overall dispersions are very different. On the left side, the Fermi crossings are close to each other, while

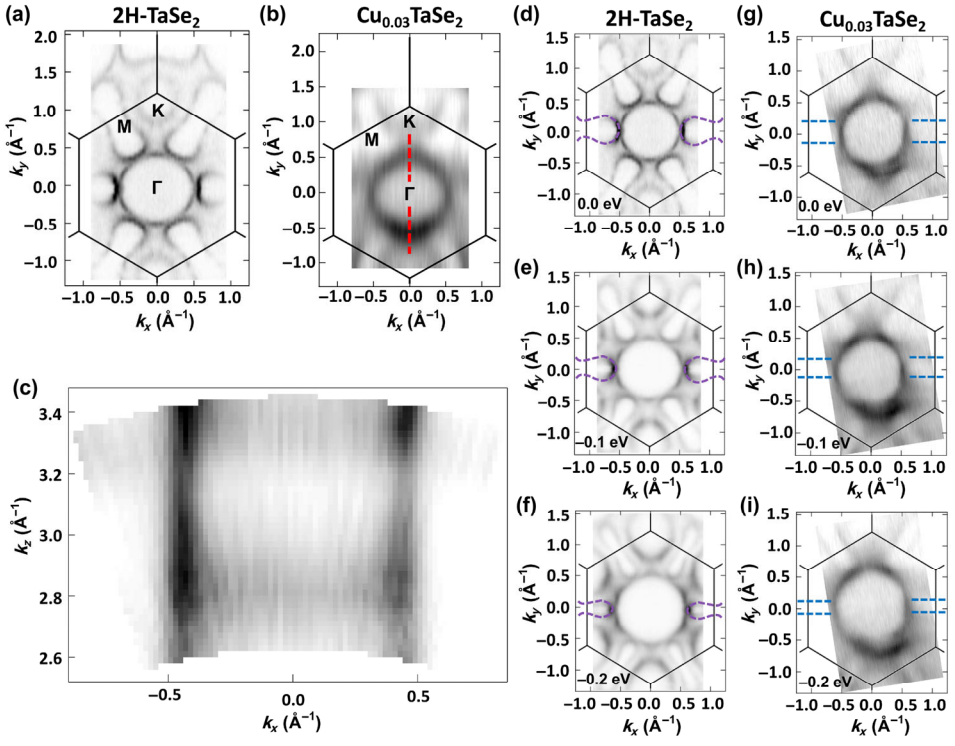

Figure 3 (a) and (b) Fermi surface topologies of $TaSe_2$ and $Cu_{0.03}TaSe_2$. The data were taken using 35 eV photons. (c) k_z dispersion along the Γ–K cut in $Cu_{0.03}TaSe_2$.The cut is marked by the red dash line in (b). The energy range is 20–50 eV and the step size is 1 eV. (d)–(f) ARPES intensity at various constant energies in $TaSe_2$. The data were taken at the Fermi level, −0.1 and −0.2 eV below the Fermi level, respectively. The purple dash lines outline the dog-bone pockets around M points in $TaSe_2$. (g)–(i) ARPES intensity at various constant energies in $Cu_{0.03}TaSe_2$. The blue dash lines outline the straight sides around M points in $Cu_{0.03}TaSe_2$.

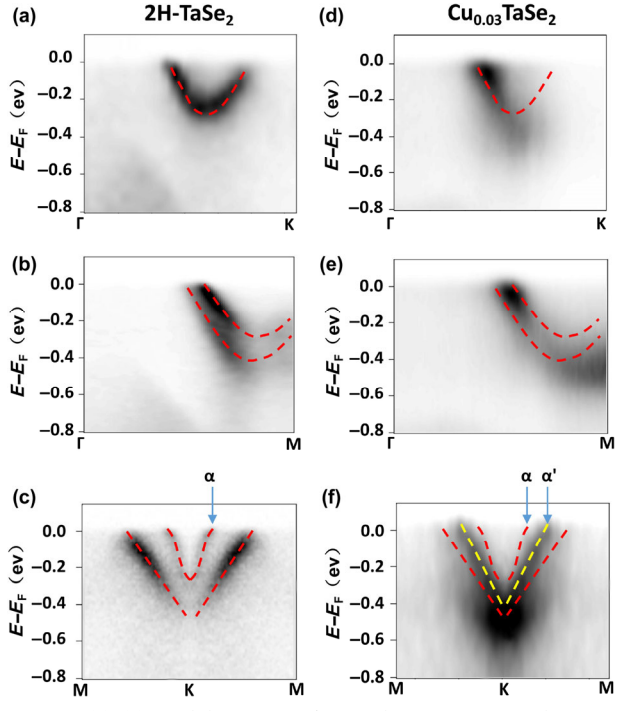

Figure 4 (a)–(c) Band dispersions of $TaSe_2$ along Γ–K, Γ–M and M–K–M directions, respectively. (d)–(f) Band dispersion of $Cu_{0.03}TaSe_2$ along Γ–K, Γ–M and M–K–M directions, respectively. The red dash lines indicate the band dispersions of $TaSe_2$.

there is a large separation in energy between the band bottoms of the parent and Cu-intercalated compounds. Figures 4(b) and 4(e) show that in the Γ–M direction the spectral weight around M in $Cu_{0.03}TaSe_2$ move to deeper binding energies after Cu intercalation. In Figs. 4(c) and 4(f), along the M–K–M direction, the band bottom shifts remarkably after Cu intercalation, while the dispersion of α band in $TaSe_2$ is different from that of α' band in $Cu_{0.03}TaSe_2$. Our data indicate that, after Cu intercalation, the overall dispersions are altered significantly. This finding is another evidence that the effect of Cu intercalation cannot be interpreted within a rigid band model with a simple electron doping. Such properties suggest that Cu intercalants interact with the host $TaSe_2$ layers and affect the fundamental band dispersions. Moreover, the variation of spectral weight after Cu intercalation is also related to the change of band structures, since the photoemission matrix element is modified by the change of electronic structures and eventually alters the spectral weight in ARPES data.

In Cu_xTiSe_2, the interactions between Se and the intercalated Cu has been investigated by first-principles calculations [26]. This study provides some insight for our understanding of the underlying mechanism in $Cu_{0.03}TaSe_2$. Theoretical studies suggest that in Cu_xTiSe_2 the chemical bonds form between the copper intercalant and neighboring Se atoms, a mild charge transfer occurs and slight increases the carrier concentration in the host layers, while the structural configurations in the host layers are not evidently affected by the Cu–Se bonds and the charge transfer [27]. All these properties are highly consistent with our observations from XAFS measurements on $Cu_{0.03}TaSe_2$.

According to our XAFS data, the Cu–Se bond length is ~ 2.4 Å, which is very close to the Cu–Se bond length in Cu_2Se [28] and $CuInSe_2$ [29]. Around the Fermi level, electronic states from Ta are dominant and the formation of Cu–Se bonds will change the charge transfer between Ta and Se and consequently alter the electronic states dominated by Ta. Therefore, we can naturally expect a variation of electronic bands in Cu-intercalated $TaSe_2$.

In van der Waals crystals, the carrier concentration of basic structural layers can be regulated through atom intercalation,

and consequently the physical properties of host materials are modulated. Whether atom intercalation alters the host layers and the band structures therein require investigations. In combination of XAFS and ARPES, we are able to depict atomic configurations in real space and illustrate electronic structures in *k*-space, and eventually evaluate how the intercalants influence the electronic properties in the functional layers of host materials. Our studies suggest that by regulating the chemical bonds between the intercalants and host layers in van der Waals crystals, the fundamental physical or chemical properties of the parent compounds could be modulated, which may lead to exotic functionalities in some materials.

3 Conclusions

In summary, we have studied the structures and electronic states in Cu-intercalated $TaSe_2$ using XAFS and ARPES. By comparing with the parent 2H-$TaSe_2$, we found that the intercalated Cu ions form chemical bonds with Se in the host $TaSe_2$ layers and a mild charge transfer occurs from Cu to $TaSe_2$ layers. Band structure measurements show that the resulting electronic structures in $Cu_{0.03}TaSe_2$ cannot be interpreted by a simple rigid band model with merely charge doping effect. Our studies suggest that the pristine band dispersions in the host layers could be regulated by the intercalants when the chemical bonds develop between the foreign ions and the anions in the host layers.

Acknowledgements

We acknowledge the financial support from the National Key R&D Program of China (No. 2017YFA0402901, 2016YFA0401004), National Natural Science Foundation of China (No. 11674296, 21727801 and 11621063), the Key Research Program of the Chinese Academy of Sciences (No. XDPB01), the Innovative Program of Development Foundation of Hefei Center for Physical Science and Technology (No. 2018CXFX002), NSFC-MAECI (51861135202).

Electronic Supplementary Material: Supplementary material (composition analysis and magnetic susceptibility measurement of $Cu_{0.03}TaSe_2$) is available in the online version of this article at https://doi.org/10.1007/s12274-020-2613-3.

References

[1] Wilson, J. A.; Yoffe, A. D. The transition metal dichalcogenides discussion and interpretation of the observed optical, electrical and structural properties. *Adv. Phys*. **1969**, *18*, 193–335.

[2] Wang, Q. H.; Kalantar-Zadeh, K.; Kis, A.; Coleman, J. N.; Strano, M. S. Electronics and optoelectronics of two-dimensional transition metal dichalcogenides. *Nat. Nanotechnol*. **2012**, *7*, 699–712.

[3] Manzeli, S.; Ovchinnikov, D.; Pasquier, D.; Yazyev, O. V.; Kis, A. 2D transition metal dichalcogenides. *Nat. Rev. Mater*. **2017**, *2*, 17033.

[4] Neto, A. H. C. Charge density wave, superconductivity, and anomalous metallic behavior in 2D transition metal dichalcogenides. *Phys. Rev. Lett*. **2001**, *86*, 4382–4385.

[5] Liu, Y.; Wang, G.; Ying, T. P.; Lai, X. F.; Jin, S. F.; Liu, N.; Hu, J. P.; Chen, X. L. Understanding doping, vacancy, lattice stability, and superconductivity in $K_xFe_{2-y}Se_2$. *Adv. Sci*. **2016**, *3*, 1600098.

[6] Hor, Y. S.; Williams, A. J.; Checkelsky, J. G.; Roushan, P.; Seo, J.; Xu, Q.; Zandbergen, H. W.; Yazdani, A.; Ong, N. P.; Cava, R. J. Superconductivity in $Cu_xBi_2Se_3$ and its implications for pairing in the undoped topological insulator. *Phys. Rev. Lett*. **2010**, *104*, 057001.

[7] Komsa, H. P.; Kotakoski, J.; Kurasch, S.; Lehtinen, O.; Kaiser, U.; Krasheninnikov, A. V. Two-dimensional transition metal dichalcogenides under electron irradiation: Defect production and doping. *Phys. Rev. Lett*. **2012**, *109*, 035503.

[8] Muhammad, Z.; Mu, K. J.; Lv, H. F.; Wu, C. Q.; ur Rehman, Z.; Habib, M.; Sun, Z.; Wu, X. J.; Song, L. Electron doping induced semiconductor to metal transitions in $ZrSe_2$ layers via copper atomic intercalation. *Nano Res*, **2018**, *11*, 4914–4922.

[9] Morosan, E.; Zandbergen, H. W.; Dennis, B. S.; Bos, J. W. G.; Onose, Y.; Klimczuk, T.; Ramirez, A. P.; Ong, N. P.; Cava, R. J. Superconductivity in Cu_xTiSe_2. *Nat. Phys*. **2006**, *2*, 544–550.

[10] Zhao, J. F.; Ou, H. W.; Wu, G.; Xie, B. P.; Zhang, Y.; Shen, D. W.; Wei, J.; Yang, L. X.; Dong, J. K.; Arita, M. et al. Evolution of the Electronic Structure of 1*T*- Cu_xTiSe_2. *Phys. Rev. Lett*. **2007**, *99*, 146401.

[11] Fang, Y. Q.; Pan, J.; He, J. Q.; Luo, R. C.; Wang, D.; Che, X. L.; Bu, K. J.; Zhao, W.; Liu, P.; Mu, G. et al. Structure re-determination and superconductivity observation of bulk 1T MoS_2. *Angew. Chem., Int. Ed*. **2018**, *57*, 1232–1235.

[12] Graebner, J. E. Fermi surface measurements in 2H-$TaSe_2$. *Solid State Commun*. **1977**, *21*, 353–356.

[13] Liu, R.; Olson, C. G.; Tonjes, W. C.; Frindt, R. F. Momentum dependent spectral changes induced by the charge density wave in 2*H*-$TaSe_2$ and the implication on the CDW mechanism. *Phys. Rev. Lett*. **1998**, *80*, 5762–5765.

[14] Rossnagel, K.; Rotenberg, E.; Koh, H.; Smith, N. V.; Kipp, L. Fermi surface, charge-density-wave gap, and kinks in 2*H*-$TaSe_2$. *Phys. Rev. B* **2005**, *72*, 121103.

[15] Borisenko, S. V.; Kordyuk, A. A.; Yaresko, A. N.; Zabolotnyy, V. B.; Inosov, D. S.; Schuster, R.; Büchner. B.; Weber, R.; Follath, R.; Patthey, L. et al. Pseudogap and charge density waves in two dimensions. *Phys. Rev. Lett*. **2008**, *100*, 196402.

[16] Ressler, T. *WinXAS*: A program for X-ray absorption spectroscopy data analysis under MS-Windows. *J. Synchrot. Radiat*. **1998**, *5*, 118–122.

[17] Ankudinov, A. L.; Ravel, B.; Rehr, J. J.; Conradson, S. D. Real-space multiple-scattering calculation and interpretation of x-ray-absorption near-edge structure. *Phys. Rev. B* **1998**, *58*, 7565–7576.

[18] Kordyuk, A. A.; Evtushinsky, D. V.; Zabolotnyy, V. B.; Haenke, T.; Hess, C.; Buechner, B.; Yaresko, A. N.; Berger, H.; Borisenko, S. V. Chiral honeycomb superstructure, parquet nesting, and Dirac cone formation in Cu-intercalated 2H-$TaSe_2$. arXiv: 1003.1976, 2010.

[19] Steigmeier, E. F.; Harbeke, G.; Auderset, H.; DiSalvo, F. J. Softening of charge density wave excitations at the superstructure transition in 2H-$TaSe_2$. *Solid State Commun*. **1976**, *20*, 667–671.

[20] Sohrt, C.; Stange, A.; Bauer, M.; Rossnagel, K. How fast can a Peierls-Mott insulator be melted? *Faraday Discuss*. **2014**, *171*, 243–257.

[21] Kumakura, T.; Tan, H.; Handa, T.; Morishita, M.; Fukuyama, H. Charge density waves and superconductivity in 2H-$TaSe_2$. *Czech. J. Phys*. **1996**, *46*, 2611–2612.

[22] Smith, N. V.; Kevan, S. D.; DiSalvo, F. J. Band structures of the layer compounds 1T-TaS_2 and 2H-$TaSe_2$ in the presence of commensurate charge-density waves. *J. Phys. C Solid State Phys*. **1985**, *18*, 3175–3189.

[23] Brauer, H. E.; Starnberg, H. I.; Holleboom, L. J.; Hughes, H. P.; Strocov, V N. Na and Cs intercalation of 2H-$TaSe_2$ studied by photoemission. *J. Phys. Condes. Matter* **2001**, *13*, 9879–9895.

[24] Ge, Y. Z.; Liu, A. Y. First-principles investigation of the charge-density-wave instability in 1T-$TaSe_2$. *Phys. Rev. B* **2010**, *82*, 155133.

[25] Yan, J. A.; Cruz, M. A. D.; Cook, B.; Varga, K. Structural, electronic and vibrational properties of few-layer 2H-and 1T-$TaSe_2$. *Sci. Rep*. **2015**, *5*, 16646.

[26] Ryu, H.; Chen, Y.; Kim, H.; Tsai, H. Z.; Tang, S. J.; Jiang, J.; Liou, F.; Kahn, S.; Jia, C. H.; Omrani, A. A. et al. Persistent charge-density-wave order in single-layer $TaSe_2$. *Nano Lett*. **2018**, *18*, 689–694.

[27] Jishi, R. A.; Alyahyaei, H. M. Electronic structure of superconducting copper intercalated transition metal dichalcogenides: First-principles calculations. *Phys. Rev. B* **2008**, *78*, 144516.

[28] Antsyshkina, A. S.; Sadikov, G. G.; Koneshova, T. I.; Sergienko, V. S. X-ray diffraction study of the Cu_2Se-In_2Se_3-Cr_2Se_3 system near $CuInCr_2Se_5$. *Inorg. Mater*. **2004**, *40*, 1259–1263.

[29] Knight, K. S. The crystal structures of $CuInSe_2$ and $CuInTe_2$. *Mater. Res. Bull*. **1992**, *27*, 161–167.